Research Square

Preprints are preliminary reports that have not undergone peer review.
They should not be considered conclusive, used to inform clinical practice,
or referenced by the media as validated information.

Biomass-Derived Carbon Quantum Dots for Wettability Alteration of Oil-Wet Carbonate Rocks: A Micromodel Flooding Study

Mohammed Sadeq Dabis
Amirkabir University of Technology
Mostafa Keshavarz Moraveji
Amirkabir University of Technology
Luma Ahmed
Al-Zahraa Center for Medical and Pharmaceutical Research Sciences (ZCMRS), Al-Zahraa University for Women
Mohammad Sharifi
m_sharifi@aut.ac.ir
Amirkabir University of Technology

Article

Keywords: Carbon quantum dots, Spent coffee grounds, Wettability alteration, Micromodel flooding, Biomass waste valorization

Posted Date: November 12th, 2026

DOI: https://doi.org/10.21203/rs.3.rs-11415490/v1

License: This work is licensed under a Creative Commons Attribution 4.0 International License.
Read Full License

Additional Declarations: No competing interests reported.

Biomass-Derived Carbon Quantum Dots for Wettability Alteration of Oil-Wet Carbonate Rocks: A Micromodel Flooding Study

Mohammed Sadeq Dabis[a], Mostafa Keshavarz Moraveji[b], Luma Ahmed[c, d], Mohammad Sharifi[a,*]

[a] Department of Petroleum and Geoenergy Engineering, Amirkabir University of Technology, Tehran, Iran

[b] Department of Chemical Engineering, Amirkabir University of Technology (Tehran Polytechnic), Tehran, Iran

[c] Al-Zahraa Center for Medical and Pharmaceutical Research Sciences (ZCMRS), Al-Zahraa University for Women, Karbala, Iraq.

[d] Department of Chemistry, College of Science, University of Kerbala, Karbala, Iraq.

* Corresponding author: Mohammad Sharifi (m_sharifi@aut.ac.ir)

Abstract

Restoring the water-wet state of oil-wet carbonate rocks through wettability alteration is one of the most effective approaches for improving oil recovery. Although conventional surfactants and nanomaterials have been widely investigated for this purpose, carbon quantum dots (CQDs) synthesized from sustainable biomass precursors have received limited attention in enhanced oil recovery applications. This study investigates the effect of CQDs derived from brewed coffee grounds on altering the wettability of oil-wet carbonate rocks and, consequently, improving oil recovery. CQDs were synthesized using a modified hydrothermal method and comprehensively characterized by X-ray diffraction (XRD), Fourier-transform infrared spectroscopy (FTIR), field-emission scanning electron microscopy (FESEM), and dynamic light scattering (DLS). Contact angle measurements demonstrated a significant reduction from 123° for untreated oil-wet rocks to 52° following treatment with a 3 vol.% CQD suspension, indicating a substantial shift toward water-wet conditions. In contrast, the CQDs showed no significant effect on the interfacial tension (IFT) between crude oil and water. Micromodel flooding experiments resulted in an incremental oil recovery of approximately 15.8% compared with DI water flooding. Overall, the results indicate that the spent-coffee-ground-derived material altered the wettability of oil-aged carbonate surfaces and improved oil recovery in the tested oil-wet micromodel.

Keywords: Carbon quantum dots, Spent coffee grounds, Wettability alteration, Micromodel flooding, Biomass waste valorization.

1 Introduction

Despite the rapid growth of renewable energy technologies, crude oil remains one of the world's primary energy resources and an indispensable feedstock for the petrochemical industry. Consequently, improving the recovery of existing oil reservoirs has become increasingly important to meet growing energy demand while reducing the need for new field developments. Oil reservoirs are subsurface porous rocks containing interconnected pores and pore throats in which crude oil is stored. For crude oil to be produced, it must flow through these extremely small pores and tortuous paths; however, a significant fraction of the oil becomes trapped within the fine voids because of capillary forces [1-3]. To recover this residual oil, enhanced oil recovery techniques have been developed and commonly divided into secondary and tertiary recovery [2, 4, 5].

Briefly, secondary recovery involves actions that displace oil through the reservoir rock by increasing pressure and pushing the oil with viscous forces, including waterflood methods and gas injection under immiscible conditions [6, 7]. By contrast, tertiary methods rely on changing fluid–fluid or rock–fluid interactions (i.e., interfacial tension (IFT) and wettability) to mobilize the trapped oil [8, 9].

The wettability of the rock refers to which fluid the rock prefers to be wetted by when two or more immiscible fluids are present [1, 10, 11]. In oil reservoirs, water and oil always coexist within the pores, and their distribution depends on rock–fluid interactions. If the rock prefers oil as the wetting phase, it is oil-wet, and the oil will stick more strongly to the pore walls, leading to greater trapping compared to water-wet rocks. Therefore, water-wet reservoirs generally allow a higher percentage of the oil to be recovered. Wettability can be altered to become more water-wet, thereby reducing the amount of trapped oil and increasing recovery by injecting specific fluids [12, 13].

Many kinds of injecting fluids could be used in order to alter the wettability of the rock and consequently increase the recovery. These fluids including low saline water, surfactant, alkaline, foam, and nano fluids [14]. These nano fluids may change the wettability and the IFT, which may lead to increased oil recovery as reported in literature. But some researchers found that when the nano fluids have been injected in the core, they agglomerated in the throats and may plug the paths as reported by Kuang et al. [15]. Carbon quantum dots (CQDs) have attracted interest as potential EOR additives. However, their suitability for transport through porous media depends on their size and dispersion behavior under the conditions of use. CQDs also show fluorescence properties under ultraviolet (UV) light, making them applicable in medicine, optical devices, tracer sensors, biosensing, cell imaging, the study of biological processes in living cells, and drug delivery [16-20]. On the other hand, CQDs have been recently studied in the petroleum industry as drilling fluid additives and as agents for enhanced oil recovery.

The precursors used to synthesize CQDs in enhanced oil recovery (EOR) research are mainly chemicals such as graphite and citric acid. The most common synthesis method is the hydrothermal process in the presence of urea or ethylenediamine, under thermal conditions spanning 130–200 °C, and reaction times between 3 and 10 hours [21, 22].

Several studies have reported that CQD treatment can shift rock wettability toward a more water-wet state. Water flooding with CQDs in limestone cores resulted in a shift toward a water-wet condition, although no significant change in IFT was observed in some cases [23-25]. Functionalized CQDs, including benzene sulfonate-modified carbon dots, have also demonstrated wettability alteration and reduced oil–rock adhesion [26-29]. These findings suggest that CQDs can modify the rock–fluid interactions that control wettability.

The reported effects of CQDs on interfacial tension (IFT), however, are not consistent among studies. Some CQD formulations have been reported to reduce both IFT and contact angle [21, 27], whereas other studies have reported significant IFT reduction without investigating the corresponding effects on wettability or oil recovery [30]. These findings indicate that wettability alteration may occur independently of a significant reduction in IFT, depending on the CQD formulation and experimental conditions.

The effect of CQDs on oil displacement has also been investigated through core and micromodel flooding experiments. Previous core flooding studies have demonstrated that CQDs and functionalized CQDs can improve oil recovery, with reported improvements ranging approximately between 14.4 and 28% and varying considerably depending on CQD composition, surface modification, and experimental conditions [21, 26-29].

In addition to their application in oil displacement, the stability of CQDs under reservoir-relevant conditions has also been investigated. CQDs synthesized from citric acid and ethylenediamine were reported to remain stable under high temperature and pH conditions and were proposed for tracer applications [22].

Overall, the literature suggests that CQDs are a promising class of nanomaterials for EOR. This is due to their small size which may reduce the risk of pore plugging, their stability which may provide stability under different reservoir conditions, as well as their surface chemical characteristics which can be adjusted to improve wettability and interfacial properties. However, most reported CQDs for EOR have been synthesized from conventional chemical or carbonaceous precursors, while the use of waste biomass as a precursor remains comparatively underexplored. In addition, pore-scale investigations of biomass-derived CQDs in porous media remain limited, particularly for oil-wet carbonate systems. In particular, the use of waste biomass as a precursor for CQDs in EOR remains comparatively underexplored. From an environmental perspective, converting spent coffee grounds into functional carbon nanomaterials provides a potential route for valorizing an abundant organic waste stream while reducing the need for additional carbonaceous precursors. In this paper, CQDs are synthesized from spent coffee grounds by a simple procedure. Micromodel flooding experiments are used to investigate the enhance oil recovery.

Therefore, this study investigates the potential of biomass-derived CQDs synthesized from spent coffee grounds to alter the wettability of oil-wet carbonate surfaces and improve oil recovery. The effects of CQD concentration on wettability alteration and interfacial tension are evaluated, followed by pore-scale flooding experiments using an oil-wet micromodel to assess the resulting oil-recovery performance.

2 Experimental

2.1 Synthesize CQD

In this work, spent coffee grounds have been used as natural resource to synthesize the carbon quantum dots. This spent coffee grounds gathered from a local coffee shop, dried in the oven at the temperature of 60 degrees Celsius. To synthesize the carbon quantum dots we used a modified solvothermal method based on several literatures [22, 30-34]. Five grams of this spent coffee grounds were added to 60 ml of deionized water. After stirring for about 10 minutes the 0.4 ml of the ethylene diamine and 0.1 g of powder Sodium dodecyl sulfate (SDS) surfactant was added to solution. After the solution be homogenized, it was put in the vessel of Teflon of autoclave to be held in the oven in temperature of 170 degree for 5 hours and let it time to be cold to the ambient temperature. The solution color after synthesis was dark brownish, that contains carbon quantum dots and other unwanted components that must be eliminated.

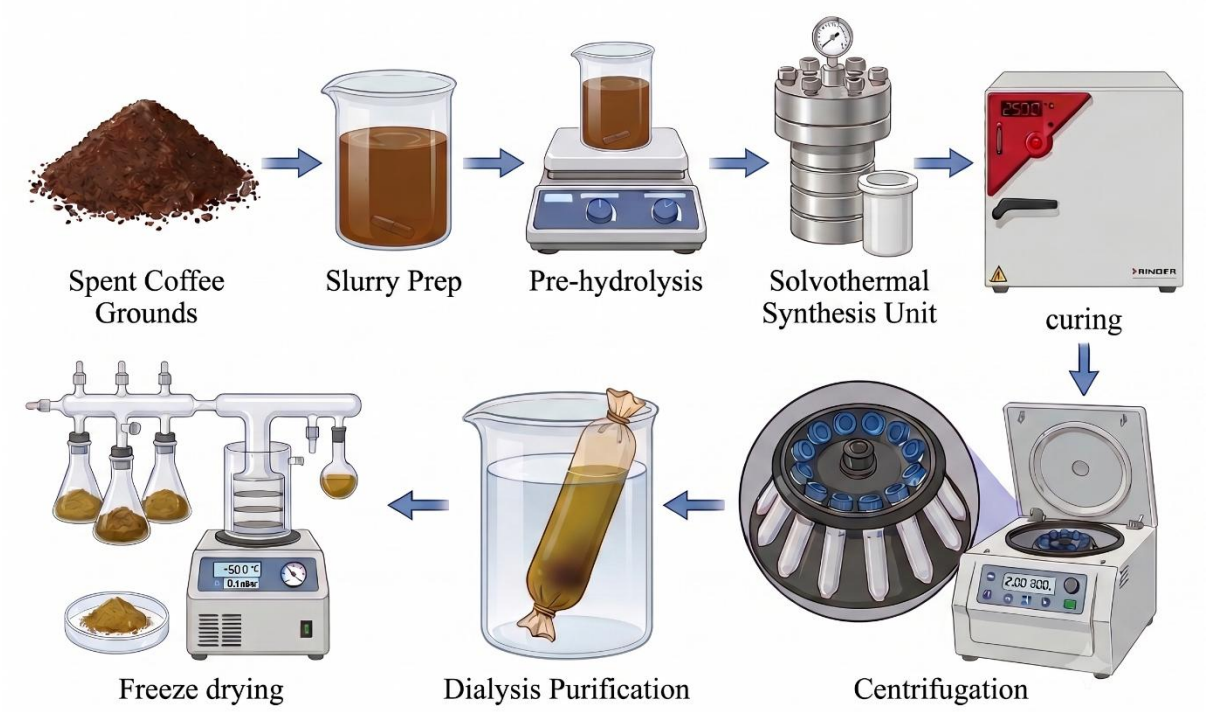


Figure 1 CQD synthesis of spent coffee grounds includes following steps: magnet stirrer, hydrothermal process, separation by centrifuge, dialysis bag, and freeze drying.

The main step in preparing the CQDs is the purifying the fine particles in scale of below the 10 nm from the larger particle that may be presence in the final solution after the synthesis step. The purification step consists of several methods to separate the CQDs of the solution including the separation by centrifuge, filtering by syringe filter, purifying by dialysis bag and finally freeze-drying processes. The dark brownish solution first centrifuged by the speed of 12000 rpm for the 20 minutes in the room temperature. The supernatant includes most of CQDs in contrast the pellet contains the larger particles. In fact, the supernatant separated and the large particles remain in the pellet diluted by the DI water and centrifuged again in the same conditions. This supernatant is again separated and be added to that supernatant prepared from the first centrifugation but the pellet in this step be abandoned. Care must be taken when the

supernatant be separated not to inter any large particle of pellet to the supernatant. In this step in the supernatant includes not only the CQDs particles but also contains larger particles that it must be disposed of. After centrifuge process, it is necessary that the supernatant to be filtered by using syringe filter of 0.22 μm to ensure the large particles have been eliminated. Then, the CQDs that exists in supernatant, was separated by employing a dialysis bag having Molecular weight cut-off (MWCO) of 1 kDa until the solutions color in the inside and the outside of dialysis bag be the same. It took about five days but it may need more depending on the concentration differences between inside and outside of dialysis bag. The fluid passes the dialysis bag contains fine particles containing unreacted materials and some quantity of carbon quantum dots but the large particles remain inside of dialysis bag. This final solution contains CQDs freeze dried for analyzing purpose like imaging by field emission scanning electron microscope (FESEM) or FTIR be extracted as powder particles. This step can be bypassed for subsequent material preparations within this study by using the final solution directly for the designated IFT, contact angle and flooding tests, eliminating the need for vaporization.

2.2 Characterization Techniques

The characterization of CQD has performed using variety of analyses to establish their complete structural, chemical, hydrodynamic, and morphological profile. The crystal structure, phase transitions, and core crystallite dimensions of both the raw precursor and the synthesized carbon quantum dots were investigated by X-ray diffraction (XRD) using a GNR Explorer (Italy) X-ray diffractometer. The instrument was operated in a 2θ locked configuration with a Cu-Kα radiation source (wavelength = 1.5406 Angstroms) at room temperature (25 °C), scanning across a 2θ range from 9.9° to 80.0° with a step size of 0.010 degrees and a counting time of 1.0 second per step. The surface functional groups and chemical structure of the synthesized material were analyzed via Fourier-transform infrared (FTIR) spectroscopy on a Shimadzu FTIR spectrometer (Shimadzu IRAffinity-1S, Japan) using the LabSolutions IR software suite over a wavenumber within the 4000 to 400 cm^{-1} range at 4 cm^{-1} resolution. The Zeta potential and hydrodynamic size distribution of the samples were measured at 25 °C using a Nanotrac Wave II dynamic light scattering (DLS) analyzer (Microtrac MRB, USA). Before these measurements, 1 kDa dialysis membrane was used to remove unreacted precursors and low-molecular-weight impurities from the aqueous suspension. We examined the surface morphology of the dried CQD by employing a TESCAN MIRA3 FESEM (TESCAN, Czech Republic) at an accelerating voltage ranging between 5-15 kV, following sample preparation via drop-casting onto a clean substrate and subsequent gold/platinum sputter coating. By visual observation under a commercial laboratory ultraviolet (UV) lamp at an excitation wavelength of 365 nm, qualitative verification of the photoluminescence properties of the synthesized suspension was attained.

2.3 Rock Samples Preparing

Studying the effect of CQD fluids on the wettability habits of carbonate rocks is done through taking plugs from outcrop rock before slicing them into samples with thickness of about 4 mm. Deionized (DI) water was used for cleaning before the slices were dried in an oven.

The initial wettability of the cleaned slices was investigated by measuring the contact angle formed by crude oil droplet on the slice surrounded by DI water, which showed a value of approximately 30°, indicating strongly water-wet behavior. This was expected since the samples were collected from an outcrop and not exposed to reservoir fluids.

Because carbonate reservoir rocks are generally oil-wet or mixed-wet [35-37], the outcrop samples were subjected to an aging process to be in oil-wet conditions. For this purpose, the slices were washed, dried, and then immersed in crude oil from southern Iran to saturate the pores and then placed in an oven at 70 °C for seven days. Preliminary tests showed that this duration was sufficient to achieve wettability alteration. After aging, the contact angle increased from 30° to 123°, confirming that the samples had become strongly oil-wet as Figure 2 shows.

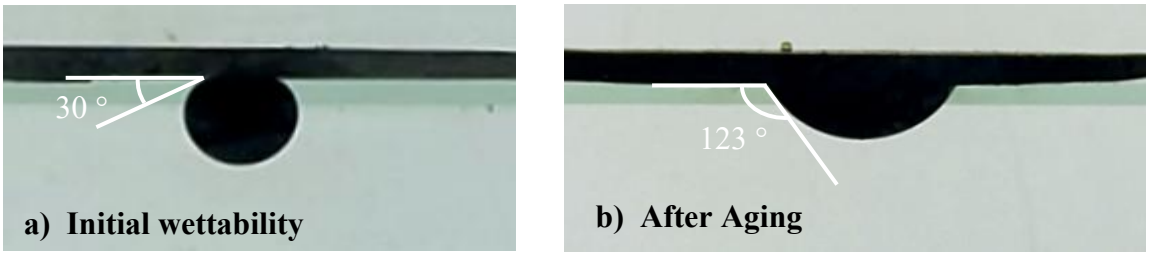


Figure 2 Contact angle of carbonate rock, (a) before aging that initial wettability is strongly water-wet with contact angle of 30 degree, (b) after aging with crude oil make the rock strongly oil-wet with contact angle of 123 degree.

2.4 Static test on wettability and IFT

The aged carbonate rock is used to identify the effects of CQDs on the wettability by using contact angle test in different concentrations. The interfacial tension test was also run using droplet pendant method in ambient conditions.

2.4.1 Contact Angle

The contact angle tests run for synthesized CQD in different concentration of 0.5% to 5%. In these experiments the aged carbonate rock slices wetted in nano fluid for 4 days to let the CQDs enough time to change the wettability of rock if it could. The test is repeated three times to ensure of the validity of the results. The contact angle is analyzed by using ImageJ image processing software with the plugin named “drop_analysis” [38]. It should be noted that the reported contact angles were measured through the aqueous phase containing CQDs, with the crude oil forming the droplet surrounded by the aqueous phase. Thus, the measured angle represents the angle between the aqueous phase and the solid surface at the three-phase contact line, rather than the angle between the crude oil phase and the surface. Accordingly, a contact angle approaching 0° indicates a strongly water-wet surface, whereas an angle approaching 180° indicates a strongly oil-wet surface.

2.4.2 Interfacial Tension Measuring

Several approaches may be used to measure the interfacial tension between two immiscible fluids. The method that is used in this work is pendant droplet that in which the crude oil injected upward in presence of DI water containing CQDs. The calculation is based on the density difference of the two immiscible fluids multiplied by gravitational acceleration, size and shape of the droplet just before the droplet detach the needle as equation derived by

Andreas et al. [39]. For processing the image, open-source software so called FIJI (or ImageJ) is used. Interfacial tension was measured using the Drop Analysis plugin, Pendant Drop sub-module developed by Daerr and Mogne [40]. In this research needle used with outer diameter of about 0.65 mm that be introduced as the scale in the FIJI software to calculate the dimensions.

Calibration has be done by using well known IFT to ensure the procedure is accurate. Air bubble in deionized water is used for calibration purpose. The IFT of air and DI water in ambient conditions is reported in the articles as approximately of 72.8 mN/m [41-43]

2.5 Fabrication of Oil-Wet Glass Micromodel

In this study, two glass micromodels with different geometries were used. The first micromodel was a simple single pore, employed to validate the process of altering glass wettability from water-wet to oil-wet. While micromodels can represent reservoir rock, they do not capture all of its characteristics. Their main advantage is transparency, which enables direct visualization of flow within porous medium. To fabricate the glass micromodel, two borosilicate glass plates with dimensions of 8 × 12 cm and 6 mm thick were employed. One of the glasses was dry-etched using a laser, based on a pattern designed with a sketching program. After cleaning and drying the two glasses to remove any contamination, surface functionalization was carried out before placing them in the furnace.

Since the surface of glass is primarily water-wet, a modified version of the process presented by Romero [44] was used to alter the wettability of the glass to oil-wet. Romero's process is based on flooding a previously fabricated glass micromodel. In contrast, we suggest performing surface functionalization during fabrication, specifically before fusing the two glasses together, which makes the coating on the glass surface stronger. In this method, a solution was prepared with a fraction of 2 to 100 of trichloromethylsilane in toluene, and the etched glass was coated for about 5 minutes until a thin film was formed on the channels.

Finally, the two glasses were placed in the furnace, and the temperature was gradually increased to 670 °C and maintained at this final temperature for 20 minutes. Care must be taken not to open the furnace door until the temperature has cooled to near room temperature, to prevent the glasses from breaking.

2.6 Micromodel Flooding Setup

Flooding tests were performed on a micromodel with complex geometry that represent a porous medium with oil-wet wettability. The setup used in this test contains a syringe pump, valves, micromodel, camera, light and tubes as illustrated in the Figure 3.

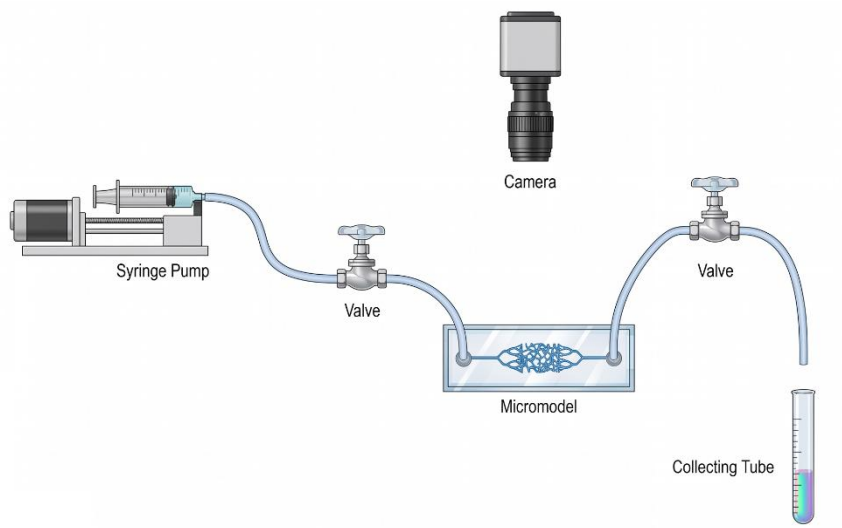


Figure 3: Schematic of setup used to flooding the micromodel.

The micromodel flooding test steps are as follows. First, the micromodel was filled with DI water and then crude oil was injected into it. This process is to mimic what happens in reality to the reservoir rock. In fact, the pores of the reservoir rock initially contain just water and then the oil migrates to rock displacing most of the existing water while some amount of this water remains within the pores, which is referred to as the connate water. Here, we replicate the same process in the laboratory so that the constructed micromodel is in conditions similar to what happens in the reservoir rock.

3 Results and Discussion

3.1 Characterization of biomass-derived CQDs

3.1.1 X-ray diffraction (XRD)

X-ray diffraction (XRD) analysis, a standard method confirming carbonaceous framework ordering, was used to investigate structural changes, phase alterations, and crystallographic configurations tracing the conversion of the raw biomass precursor to the final nanoproduct [45]. Figure 4 shows a characteristic crystalline-to-amorphous model of the XRD diffraction pattern of the raw dry coffee grounds reflecting unmodified lignocellulosic biomass structures [46]. This spectrum is seen by a distinct, broad reflection centered between $2\theta = 20°$ and 23°, which is assigned to the (002) lattice plane of the semi-crystalline cellulose fragments which is natural to the organic matrix of the brewed coffee waste [47]. This proves that the carbon atoms remain trapped within the highly organized biopolymer chains of the raw material before processing [46].

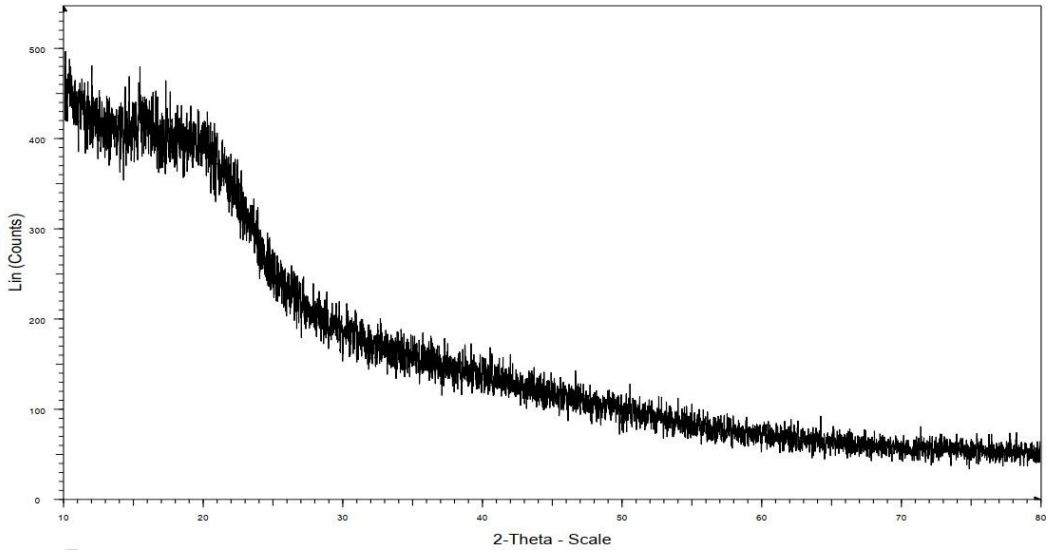


Figure 4 XRD of dried raw spent coffee grounds.

After the production steps, XRD spectrum of the final product in Figure 5 displays a substantial structural changes, which suggests the fact that the hydrothermal activity rearranged the precursor framework [48]. The localized cellulosic reflections disappeared completely and was replaced by highly diffused, single, and broadened asymmetric diffraction peak centered at approximately $2\theta = 22.5$ degrees, depicting the hallmark structural footprint of disordered graphitic networks [48].

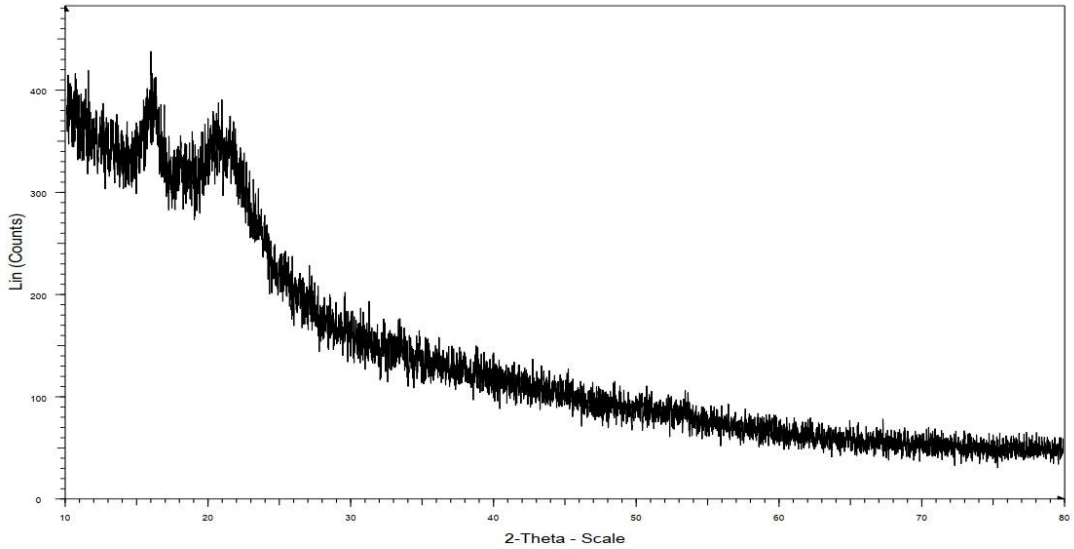


Figure 5 XRD for spent coffee grounds after hydrothermal processing.

This classic peak broadening of carbonaceous nanomaterials indicates the presence of highly disordered, amorphous sp^2 carbon networks and is reported earlier in other papers [48]. This property confirms the desirable transformation of the organic biomass into the new stable graphitic aromatic cores [48]. Basically, the severe line broadening acts as an indirect and good quantitative proof of the ultra-fine primary particle zoning, a physical property reported by

Scherrer-derivation [49]. This can be attributed to the fact that individual quantum dot cores remain below the spatial resolution limits of conventional solid-state imaging techniques like FESEM. The average crystallite domain size was estimated using the Scherrer equation. The full width at half maximum (FWHM) of the broad (002) graphitic reflection indicates that the average crystallite size is in the sub-5 nm range [48]. This mathematical derivation provides physical confirmation for the manuscript: while subsequent characterizations reveal that these CQDs assemble into stable hydrodynamic clusters when suspended in water or cast onto surfaces, their underlying primary core fragments are mainly bounded below the crucial 10 nm threshold [48]. While these broad diffraction features confirm the formation of disordered carbonaceous nanostructures, Scherrer calculations provide an estimate of primary crystallite domain size rather than independent proof of particle core dimensions or quantum confinement.

3.1.2 Fourier-transform infrared (FTIR) spectroscopy

Identifying surface functional groups and chemical bonds responsible for stability of the ultra-fine cores was achieved via Fourier-transform infrared (FTIR) spectroscopy using a Shimadzu FTIR system. The resulted transmission spectra, shown in Figure 6, illustrates a range of aromatic, oxygen-containing functional groups, creating an advantageous aqueous dissoluble biomass-derived nanomaterial with no need for surfactants [50].

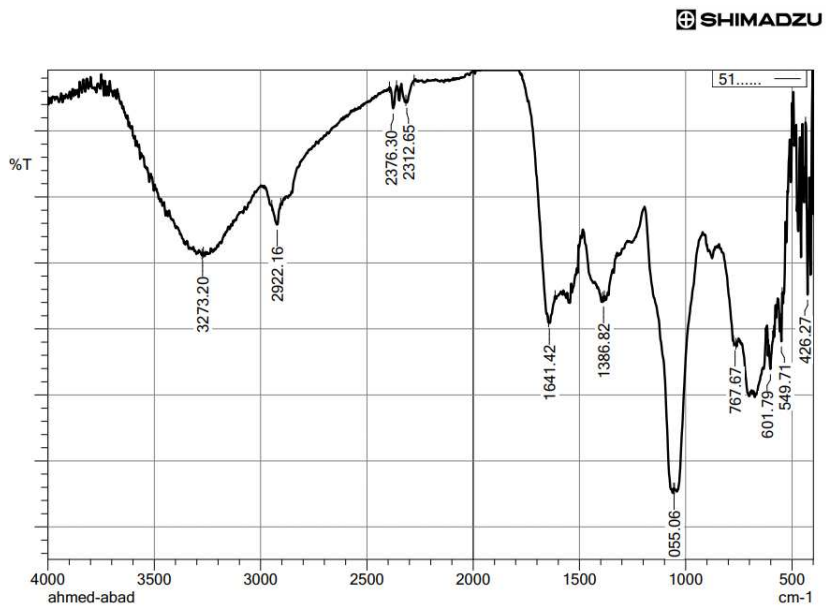


Figure 6 FTIR results of synthesized CQD of spent coffee grounds.

A broad absorption band centered near 3270 cm^{-1} reflects the presence of hydroxyl group stretching vibrations, hydrogen bounded water molecules and surface hydroxyl groups [51]. These groups improve hydrophilic properties and strengthen the interaction with water molecules hence reducing particle collection in aqueous media. A peak observed near 1640 cm^{-1} is contributed to C=C stretching vibrations of aromatic domains and/or H–O–H bending vibrations of adsorbed water molecules, which usually present in carbonaceous and biomass-derived materials [50, 52]. This traits explains how conjugated sp^2-hybridized carbon structures from carbonating brewed coffee grounds. Additional bands in the fingerprint region (1400–1000 cm^{-1}) are associated with C–O and C–O–C stretching vibrations which reflect the

presence of alcohols, ethers, and ester-like oxygenated functional groups [50, 51]. The presence of these groups suggests incomplete retention and/or formation of oxygen-containing groups during hydrothermal and carbonizing processes. These chemical modifications result in stability in aqueous fluids and reduce the possibility of aggregation in salty environments and this is advantageous in oil reservoir systems.

3.1.3 Dynamic light scattering (DLS) and zeta potential

Dynamic light scattering (DLS) is used to estimate the hydrodynamic dimensions of CQD in the water. Zeta potential measurements were used to evaluate the colloidal behavior and electrokinetic stability of nanomaterial in aqueous media [53]. As summarized in Table 1, the number-weighted mean hydrodynamic diameter of the purified suspension was 44.6 nm, whereas the volume-weighted and intensity-weighted mean diameters were measured at 92.5 nm and 139.6 nm, respectively, with a low polydispersity index (PDI) of 0.11 [54].

Table 1 DLS and Zeta potential results of CQD solution in DI water.

Parameter	Value (average)
Result quality	Good
Mean number diameter ($M_{1,0}$)	44.6 nm
Mean intensity diameter ($M_{r,r}$)	139.6 nm
Polydispersity Index (PDI)	0.11
Zeta Potential	-25.33 mV

Considering that the crystalline core sizes of the primary carbon dots were previously estimated by XRD analysis to be below 10 nm using the Scherrer equation, the larger dimensions obtained from DLS indicate the presence of solution-phase aggregation and hydration effects rather than the actual crystalline core size [53]. Such differences are commonly observed because the dimension of particles reported by DLS represent the hydrodynamic diameter, which includes both the particle core and its surrounding solvation layer [54]. The observed enlargement in hydrodynamic size therefore suggests that the nanoparticles do not remain as completely isolated entities in water, but instead form stable supramolecular clusters through intermolecular interactions [55].

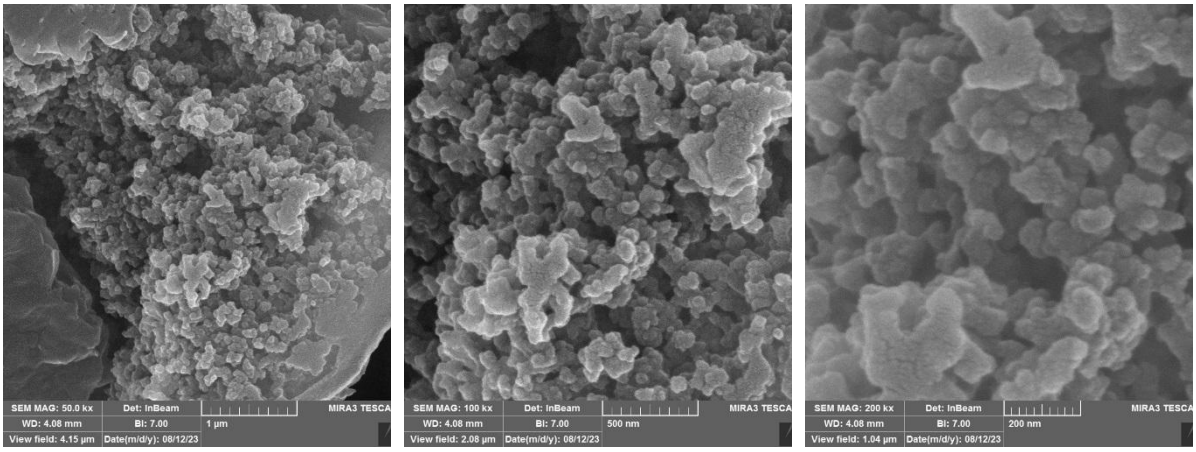
This clustering behavior can be justified by the abundant oxygen-containing surface functional groups identified by FTIR analysis, these groups include hydroxyl and carboxyl groups [56]. In aqueous environments, these polar surface groups help to form extensive hydrogen bonds with surrounding water molecules, resulting in a dense hydration shell around the nanoparticles [55]. As a result, the effective hydrodynamic dimensions become substantially larger than the crystalline core dimensions measured by XRD [53]. Moreover, the higher intensity-weighted diameter observed in DLS is consistent with the principles of Rayleigh scattering, where the intensity is strongly dependent on particle diameter, increasing in proportion to its sixth power [57], causing larger hydrated clusters to contribute inversely to the detected signal.

The low PDI of 0.11 indicates a relatively narrow particle-size distribution [54], while the zeta potential of −25.33 mV suggests electrostatic repulsion that can contribute to dispersion stability [58] under the measurement conditions.

Although the nanoparticles exist in water as hydrated supramolecular clusters rather than isolated sub-10 nm particles, their maximum hydrodynamic dimensions remain below 150 nm, as evidenced by the 90th percentile volumetric diameter of 142.8 nm. These dimensions are still considerably smaller than the typical micrometer-scale pore throat diameters (approximately 1–10 μm) commonly encountered in sandstone and carbonate reservoir formations [59]. The measured hydrodynamic dimensions are smaller than typical micrometer-scale pore throats, suggesting that the CQD dispersion has a size range potentially suitable for transport through porous media [60].

3.1.4 FESEM

To correlate the solution-phase characteristics with the solid-state morphology, FESEM images were acquired using a TESCAN MIRA3 microscope at multiple magnifications. The FESEM micrographs reveal a highly homogeneous nanostructured surface layer uniformly distributed across the substrate, with no evidence of large cracks, crystalline impurities, or uncontrolled bulk agglomeration, indicating the formation of a structurally consistent product [61]. At intermediate magnifications, the surface resolves into an interconnected network of cohesive colloidal clusters, producing pronounced nanoscale roughness and a high surface-area architecture. Such nanoscale surface texturing is considered beneficial for wettability alteration and adsorption-driven interactions in porous reservoir rocks during enhanced oil recovery (EOR) processes [62].



a) b) c)

Figure 7 FESEM images of CQDs at (a) low, (b) medium, and (c) high magnifications showing uniform nanocluster morphology.

At higher magnifications, densely packed quasi-spherical nanogranular domains are observed with lateral dimensions visually estimated within the 40–50 nm range. Although isolated carbon quantum dot cores below 10 nm are difficult to distinctly resolve in dry-state FESEM imaging due to aggregation and limited contrast in amorphous carbon networks [63], the observed cluster dimensions closely agree with the hydrodynamic diameter measured by dynamic light scattering (44.6 nm). This strong correlation confirms that the synthesized nanostructures remain confined within stable sub-micron regimes in both dispersed and dry states. From a reservoir-engineering perspective, maintaining aggregate dimensions well below typical pore-throat scales minimizes the likelihood of pore plugging, mechanical entrapment, or formation damage, supporting the suitability of these nanoclusters for transport through sandstone and carbonate porous media during EOR operations [64].

3.1.5 Optical properties

The synthesized carbon quantum dots (CQDs) displayed a light-yellow, highly transparent appearance under ambient light, confirming the formation of a well-dispersed and aggregation-free aqueous colloid (Fig. 9a). Upon UV irradiation (λ = 365 nm), the dispersion exhibited strong and uniform blue fluorescence (Fig. 9b), characteristic of CQD photoluminescence arising from radiative recombination at surface/defect states. The absence of visible scattering or turbidity further supports the high colloidal stability and nanoscale dispersion quality. This distinct excitation-dependent emission behavior is consistent with quantum confinement and surface-state dominated luminescence typically observed in sub-10 nm carbon nanostructures [61, 63], thereby confirming successful formation of CQDs with ultrasmall particle size.

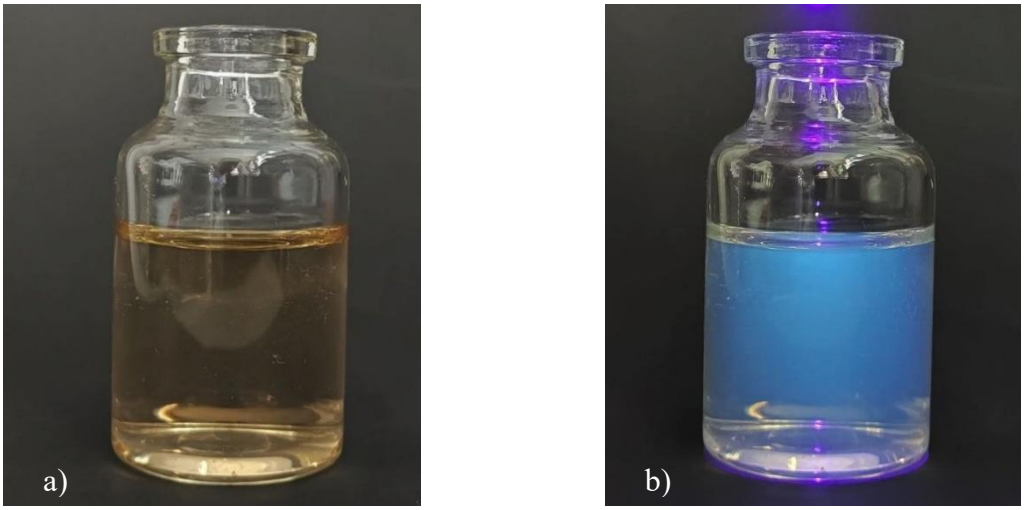


Figure 8 (a) CQD dispersion under visible light showing a clear, light-yellow colloid. (b) Under UV light (365 nm), the same sample shows strong blue fluorescence, confirming CQD formation.

3.2 Effect of CQD concentration on carbonate wettability

The concentration effect of CQD nanofluid on wettability alteration was evaluated by measuring the contact angles. The results, presented in Figure 9, demonstrate how varying concentrations influence the transition from oil-wet to water-wet conditions.

The wettability alteration behavior of carbonate rock in the presence of CQD nanofluids revealed two distinct stages. At low concentrations, the introduction of CQDs caused a sharp and rapid decrease in contact angle. Specifically, adding only 0.5 volume percent (vol.%) CQDs reduced the contact angle from 123° (strongly oil-wet) to 84°. This substantial drop at such a low dosage highlights the high surface activity of CQDs, which readily adsorb onto the carbonate surface. The trend continued as the concentration increased, with the lowest contact angle (52°) observed at 3 vol.% concentration, indicating a water-wet condition. These findings indicate that CQDs can effectively modify the surface properties of carbonate rocks, making them favorable for enhanced oil recovery processes.

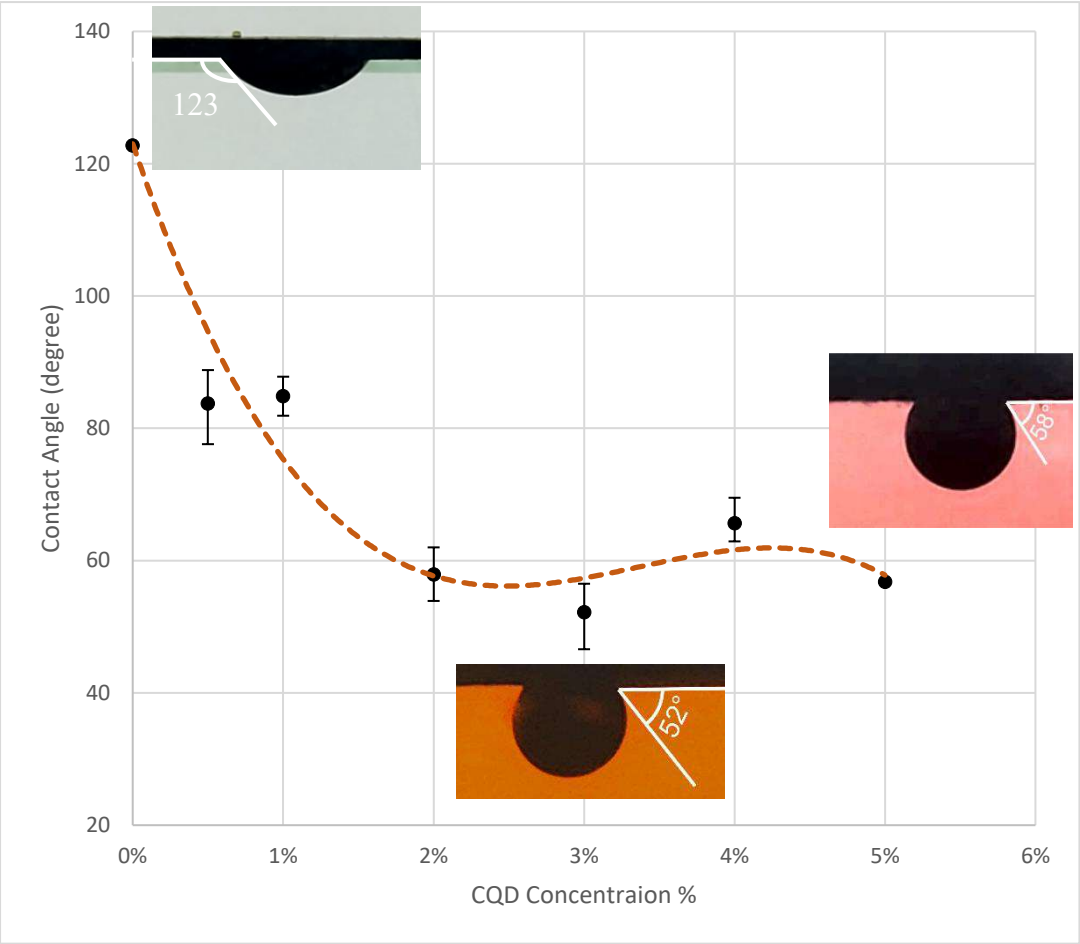


Figure 9 Concentration effect on contact angle of crude oil droplet at carbonate rock surface in presence of CQD. This graph shows clearly there is a certain concentration in which the contact angle be minimum and after this concentration, increasing of concentration has undesirable effect on contact angle.

Unexpectedly, increasing the CQD concentration beyond 3% reversed this trend slightly. Instead of stabilizing at a water-wet condition, the contact angle increased again, reaching 56–65° at 4–5 vol.%. This unwilling increase suggests that higher concentrations introduce unfavorable interactions within the nanofluid. One explanation is the aggregation of CQDs at elevated concentrations due to enhanced particle–particle attraction. Such aggregation reduces their ability to disperse uniformly and interact with the rock surface, thereby lowering their surface-modifying efficiency. Another contributing factor may be that once the surface becomes saturated with nanoparticles, additional CQDs remain suspended in the bulk solution. These suspended particles interact more with each other than with the rock surface, reducing the effective CQD–rock interaction. As a result, oil molecules regain the opportunity to adhere to the rock surface, increasing the contact angle.

Taken together, these results demonstrate that wettability alteration using CQDs is concentration-dependent. A low concentration is sufficient to induce significant wettability shifts, but there exists an optimum concentration _around 2–3 vol.%_ at which the maximum water-wet condition is achieved. Beyond this level, the wettability alteration slightly decreased, which may be associated with concentration-dependent changes in particle–rock interactions. These findings underline the importance of optimizing nanoparticle dosage, as both under-dosing and overdosing reduce efficiency.

3.3 Effect of CQD on oil-water interfacial tension

The interfacial tension between crude oil and CQD aqueous solutions was measured using the pendant drop method across CQD concentrations ranging from 0.5% to 5%. The results show no significant variation in IFT with increasing CQD concentration. The IFT values remained close to that of DI water (≈10.2 mN/m), fluctuating only slightly within a narrow range (≈8.7–11.5 mN/m), indicating that CQDs do not meaningfully influence oil–water interfacial behavior under the tested conditions.

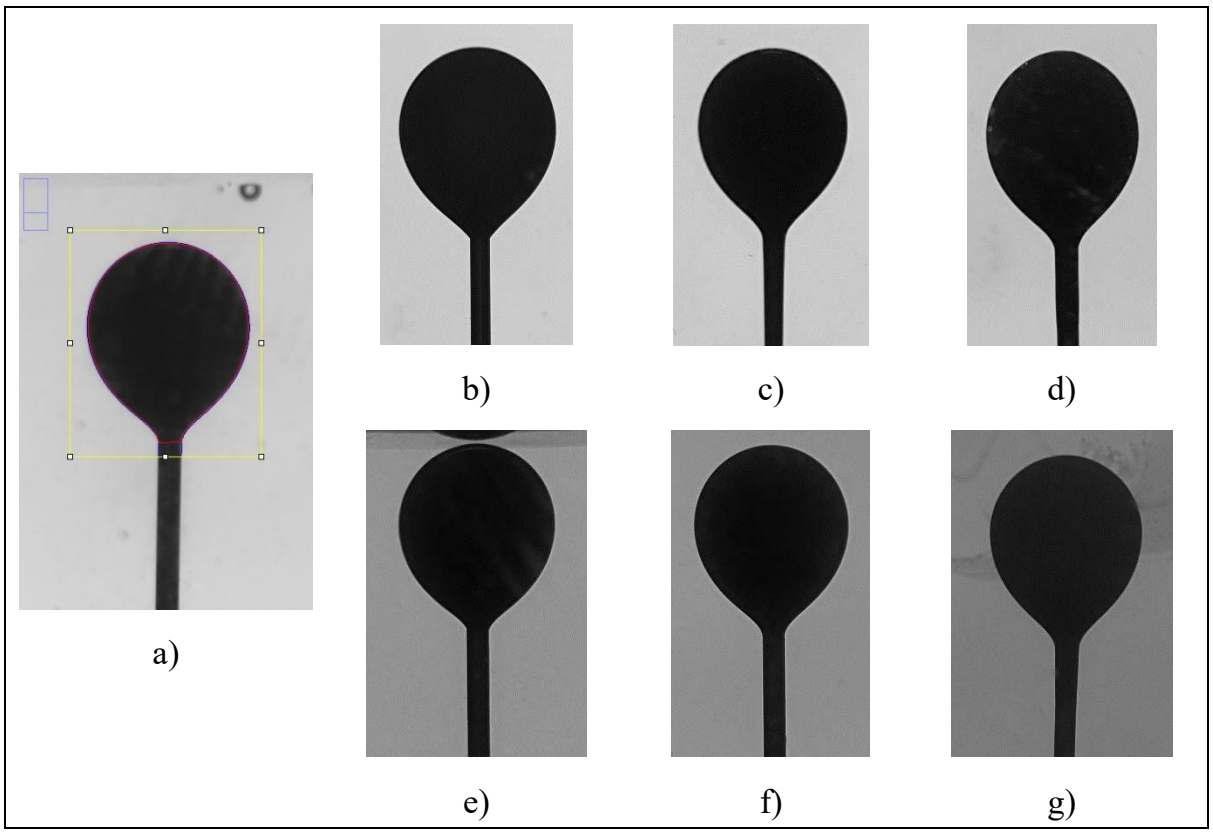


Figure 10 IFT measuring: a) The crude oil droplet within the DI water shows the IFT of 10.2 mN/m. b) to g) is the measurement of IFT at DI water containing CQDs in concentration of 0.5, 1, 2, 3, 4 and 5 vol.% respectively.

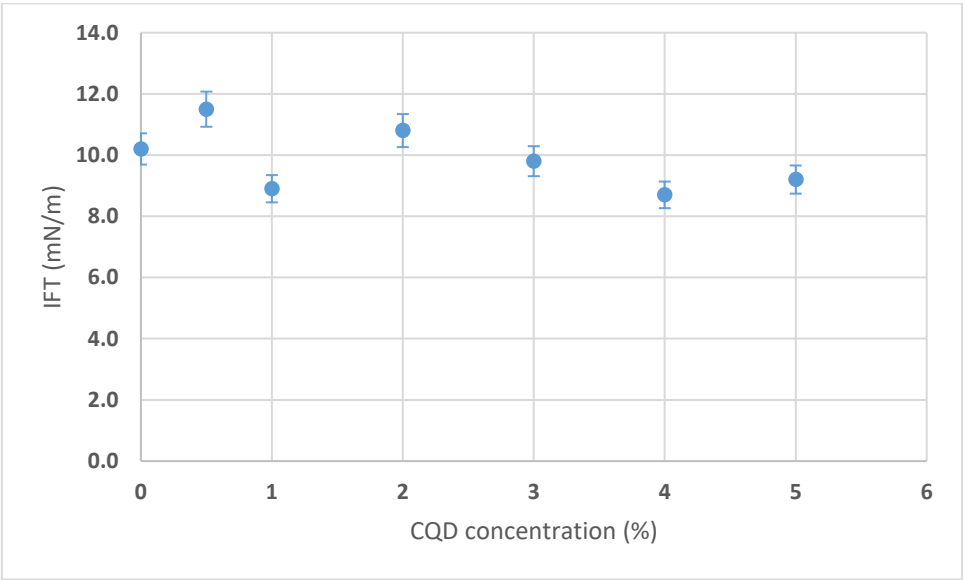


Figure 11 Interfacial tension (IFT) between crude oil and CQD aqueous solutions at different concentrations (0.5–5%), showing negligible variation compared to DI water.

3.4 Micromodel flooding

3.4.1 Establishment of oil-wet micromodel

As detailed in the micromodel fabrication section, we developed a new technique for rendering the glass surface oil-wet, which represents an improvement over the method reported by Romero [44]. The motivation for altering the surface wettability is to better replicate carbonate reservoir rocks, which are typically oil-wet. To validate the effectiveness of this method, a glass micromodel with a simple geometry was fabricated, and oil was injected into the system. As shown in Figure 12a–f, the geometry consists of three parallel straight lines with two circles on each line, allowing for simple observation and tracking of the advancing front. The oil flow patterns within the micromodel, along with the measured contact angle between the oil and the channel walls, were used to assess the wettability state. The images below illustrate the process of oil entry into the micromodel.

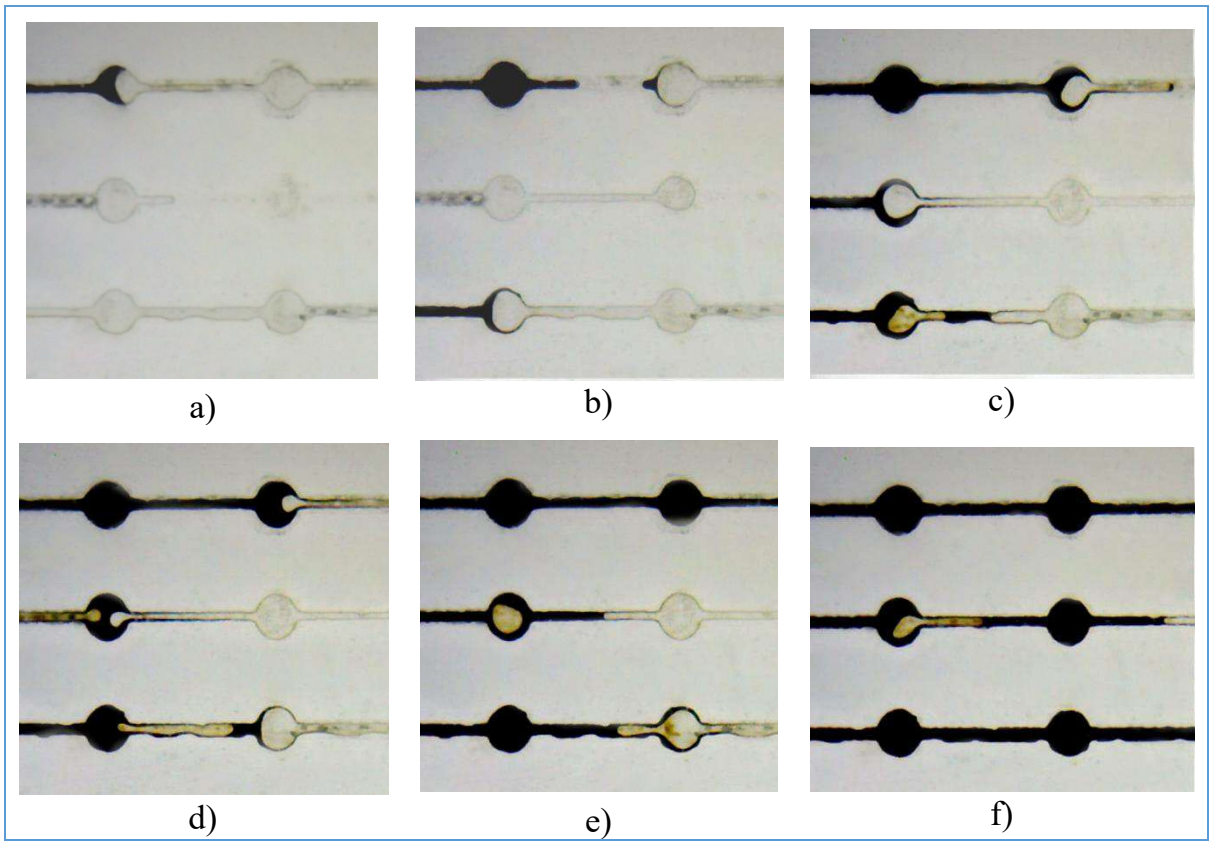


Figure 12 The process of making the micromodel oil-wet is evident, as the oil enters the micromodel from left to right.

The oil-water interface advances through the micromodel from left to right. As observed in the images, the oil adheres to the channel walls during progression, that it means the oil prefer to stick to the channel walls rather than to advance in the center of the channel as highlighted in the Figure 13. In addition, the water–oil interface concavity, oriented opposite to the direction of oil advancement, shows that capillary pressure causes the interface pressure on the water side to be higher than on the oil side. As it obvious, the pressure at the interface of the non-wetting phase is larger than the wetting phase which in fact the direction of the

concavity is the sign that the pressure at the interface of water is larger than the oil that is indicate the porous media became oil-wet successfully.

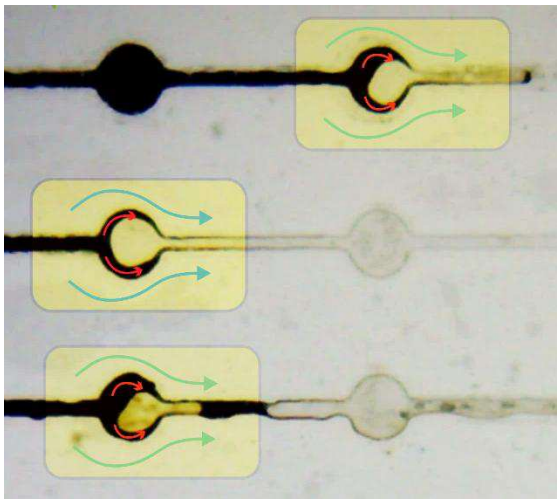


Figure 13 The advancing front tends to stick to the wall as it propagates, resulting in a concave interface opposite to the propagation direction. This clearly indicates the oil-wet wettability, as analyzed and highlighted from Figure 8c.

Furthermore, the contact angle of the oil–water interfaces with the channel walls is approximately 134°, as shown in Figure 14, which was obtained after analyzing Figure 12a. This clearly indicates that the glass micromodel was successfully modified to exhibit strong oil-wet wettability.

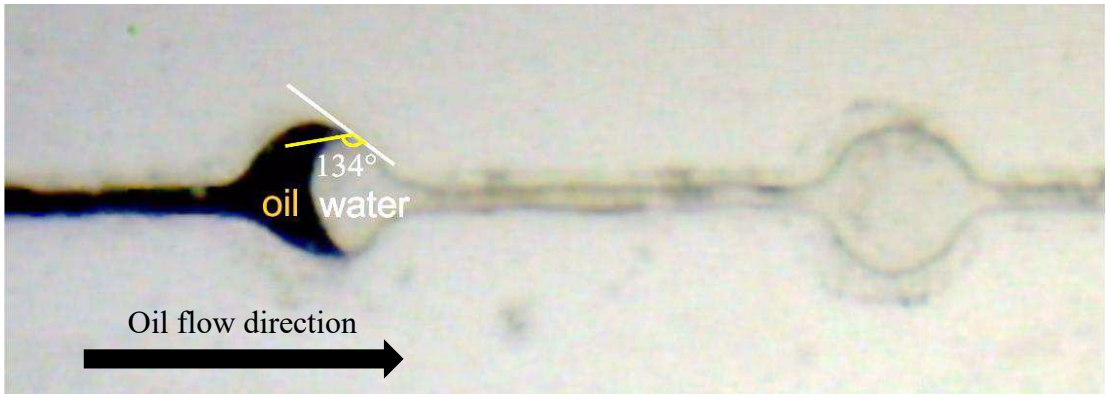


Figure 14 The contact angle is 134°, indicating that the surface modification successfully made the surface strongly oil-wet.

3.4.2 Flooding test

Then, the injection stage of water containing carbon quantum dots synthesized from the natural materials was carried out at the optimal concentration that previously obtained from the static test. As mentioned before, the lowest contact angle occurred at a concentration of 3%, which resulted in the best alteration in the wettability of the strongly oil-wet rock to water-wet. For this reason, water containing carbon quantum dots was injected at a concentration of 3%.

The injection flow rate must be selected carefully to be in the reasonable range. It is obvious that the higher the injection flow rate, the more oil is expected to be displaced from the micromodel, and the lower the flow rate, the less oil is removed from the micromodel, and this is consistent with the concept of capillary number. The capillary number represents the ratio of viscous forces that mobilize the trapped oil to capillary

forces that retain it within the pores, where velocity appears in the numerator. In fact, increasing the flow rate which means increasing in the velocity, and the higher the velocity, the higher capillary number, consequently viscous forces will dominate. So, it would be great to inject at a very high flow rate, but this flow rate has a limit and other operational considerations. Therefore, the appropriate flow rate is one that represents what is happening in the reservoir.

3.4.3 Porous micromodel

The oil-wet micromodel has been tested to evaluate the effects of fluid contains CQD on oil displacement. The micromodel that used in this study has dimensions of 11.6 × 14.8 mm and a total area of 171.7 mm^2, has a porosity area of 65.76 mm^2, with porosity of 38.3%, and oil-wet wettability.

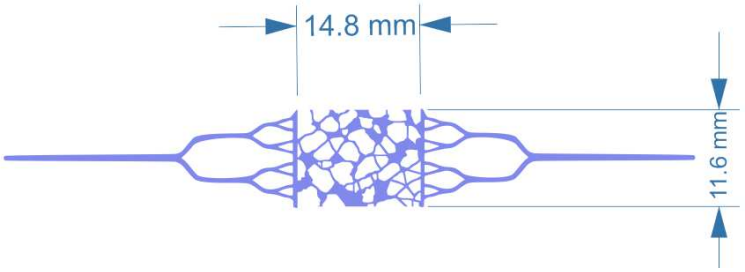
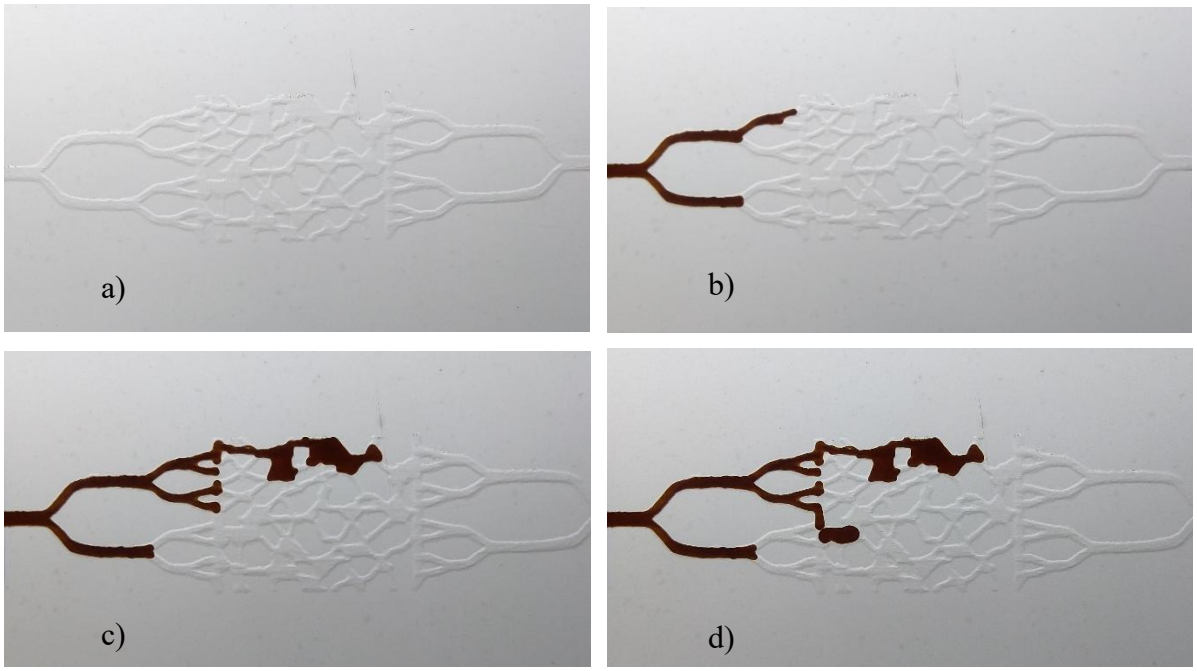


Figure 15 Micromodel design with CorelDRAW software; the length and width of the porous medium section is 14.8 and 11.6 mm respectively with porosity of 38.3%.

The flooding process was similar to the single-pore micromodel procedure described earlier, but included one additional step. First, DI water was injected into the micromodel, then crude oil was injected until the oil saturation inside the micromodel reached a constant value and did not increase further. The images below are from the oil injection stage into the micromodel containing DI water, showing how the oil displaced the water present in the pore space.



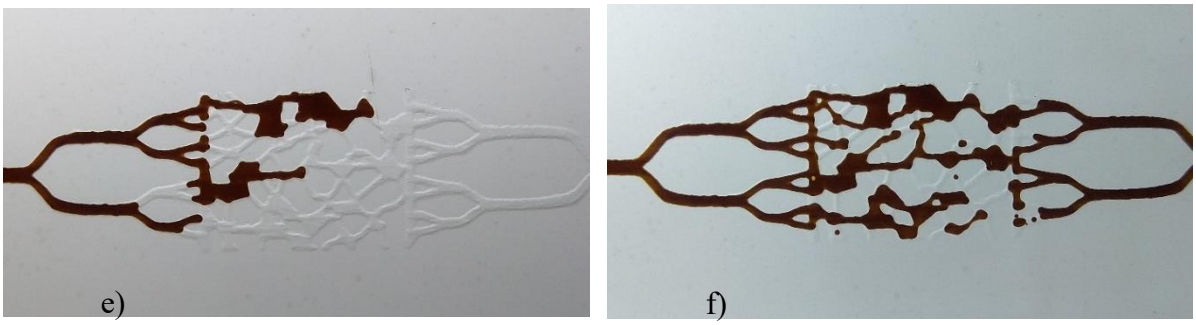


Figure 16 crude oil flooding to the oil wet micromodel; (a) initially micromodel saturated 100% of DI water, (b), (c), (d), (e) show the crude oil inter the micromodel from the left to the right and displace the initial water, (f) after crude oil injection, finally part of pores didn't invaded by the crude oil that indicated the presence of water in these pores as known as irreducible water or connate water.

After oil injection into the micromodel, which was previously 100% saturated with water, the water saturation decreases over time until it reaches an irreducible value at the end of this stage, which represents the connate water saturation. The images below show the end of the oil injection stage. At this stage, the oil area after analyzing the images was 58.45 mm^2, the porosity area 65.76 mm^2 oil saturation 88.9% and therefore the connate water saturation is 11.1%.

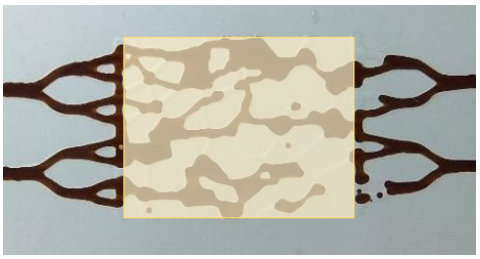


Figure 17 calculating the irreducible water saturation; the selected area is represents the porous section of micromodel, porous section of micromodel after oil injection, the crude oil is in black color and after the analyzing the area of oil is calculated to be 58.45 mm^2 that shows the oil saturation of 88.9% and the irreducible water saturation of 11.1%.

3.4.4 Baseline DI water flooding

After injecting oil into the micromodel, instead of directly injecting water containing carbon quantum dots, we first injected DI water alone to see how much the recovery would be obtained without the existence of CQDs. At this stage, we injected DI water at a flow rate of 0.075 ml/h. As the oil left the micromodel, the oil saturation decreased to the point where no further decrease in oil saturation was observed. At this point, we stopped injecting DI water. After analyzing the images, as can be seen in the images below, the area of oil remaining inside the micromodel was calculated to be 44.8 mm^2, 35.2 mm^2 and 34.2 mm^2 for injection volume of 1 PV, 1.9 PV and 2.5 PV respectively. Concerning the initial oil occupied 58.5 mm^2, therefore, the recovery factor for each pore volume injection of 1.0, 1.9 and 2.5 PV was calculated to be 23.4%, 39.9% and 41.5% respectively. The following images show the injection of DI water for 1.0, 1.9 and 2.5 pore volume.

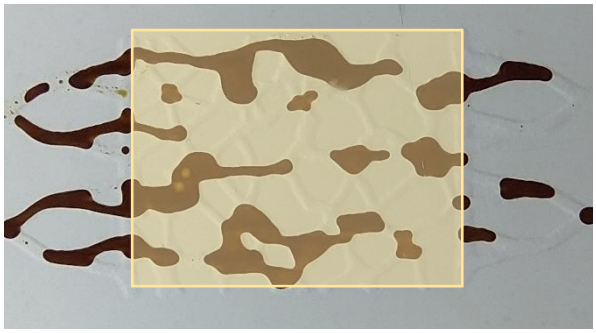


Figure 18 DI water injection in the micromodel, after processing the area occupied with the oil, black color, calculated to be approximately 44.8 mm^2 after flooding of 1.0 pore volume that show the recovery factor of 23.4% of the initial crude oil.

The Figure 19 shows the injection of DI water after 2.5 pore volume injection that leads to recovery of 41.5%.

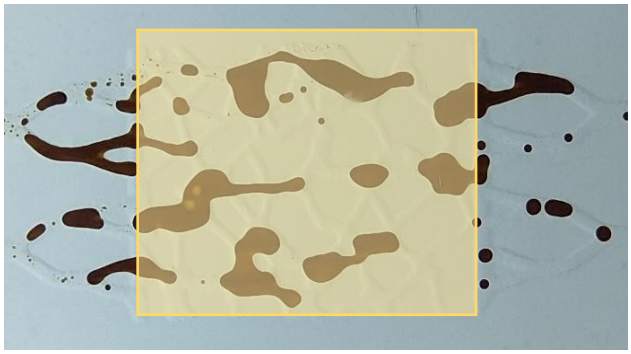
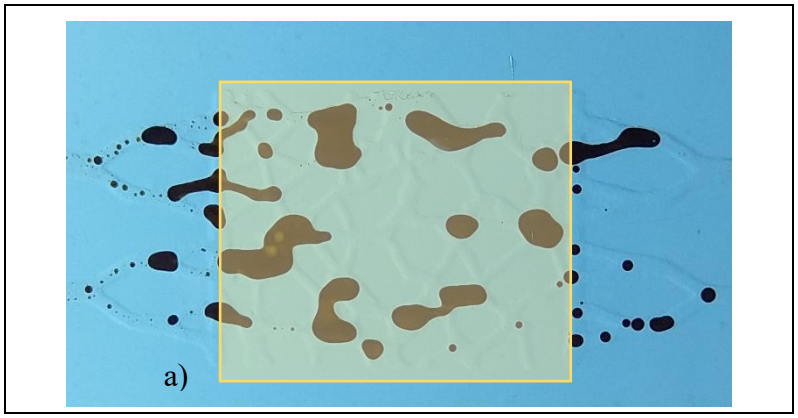


Figure 19 DI water injection in the micromodel, after processing the area occupied with the oil calculated to be approximately 34.19 mm^2 that is show the recovery factor of 41.5% approximately of the initial crude oil in the micromodel after injection of 2.5 pore volume.

3.4.5 CQD-assisted flooding

After the DI water injection stage, we started injecting water containing 3% carbon quantum dots, which showed the best change in wettability based on static tests with flow rate of 0.075 ml/h for about 6 hours. The images below are for injection at three different times, 80, 130, and 340 minutes, each of which is equivalent to 1.5, 2.5, and 6.5 times the pore volume of the porous medium, respectively. The recovery factor increased after injecting of CQD, 1.5, 2.5 and 6.5 pore volume to be 47.7%, 54.5% and 57.3% respectively. No further increase in recovery factor was observed beyond 6.5 PV.



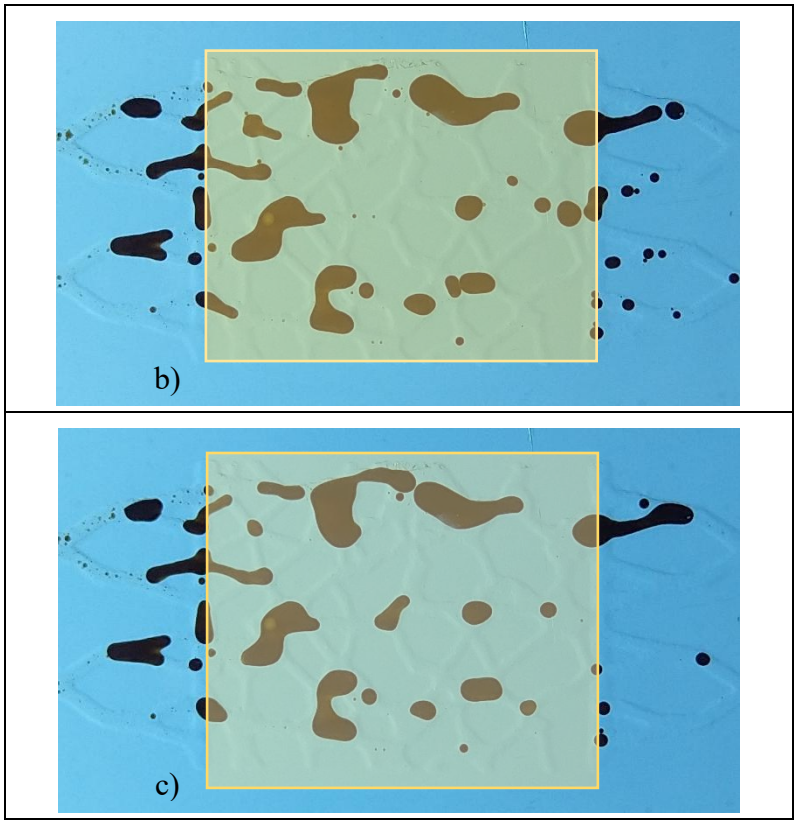


Figure 20 Recovery factor of injecting CQD; (a) 1.5 pore volume, (b) 2.5 PV, (c) 6.5 PV. The recovery factor increased after injecting of CQD, 1.5, 2.5 and 6.5 pore volume to be 47.7%, 54.5% and 57.3% respectively.

The Figure 21 shows this result of injection time on the recovery factor for the CQD. As it can be seen, as the injected volume of CQD increased the slope of the graph decreased that means the slope become more near to horizontal that means after a certain point, more volume injection of the fluid, no significant increase in recovery factor.

The injection of DI water in the earlier steps resulted in a recovery factor of 41.5%. By contrast the injection of CQD with the same flow rate of DI water injection, shows the recovery factor of 57.3% that improved by approximately of 15.8%.

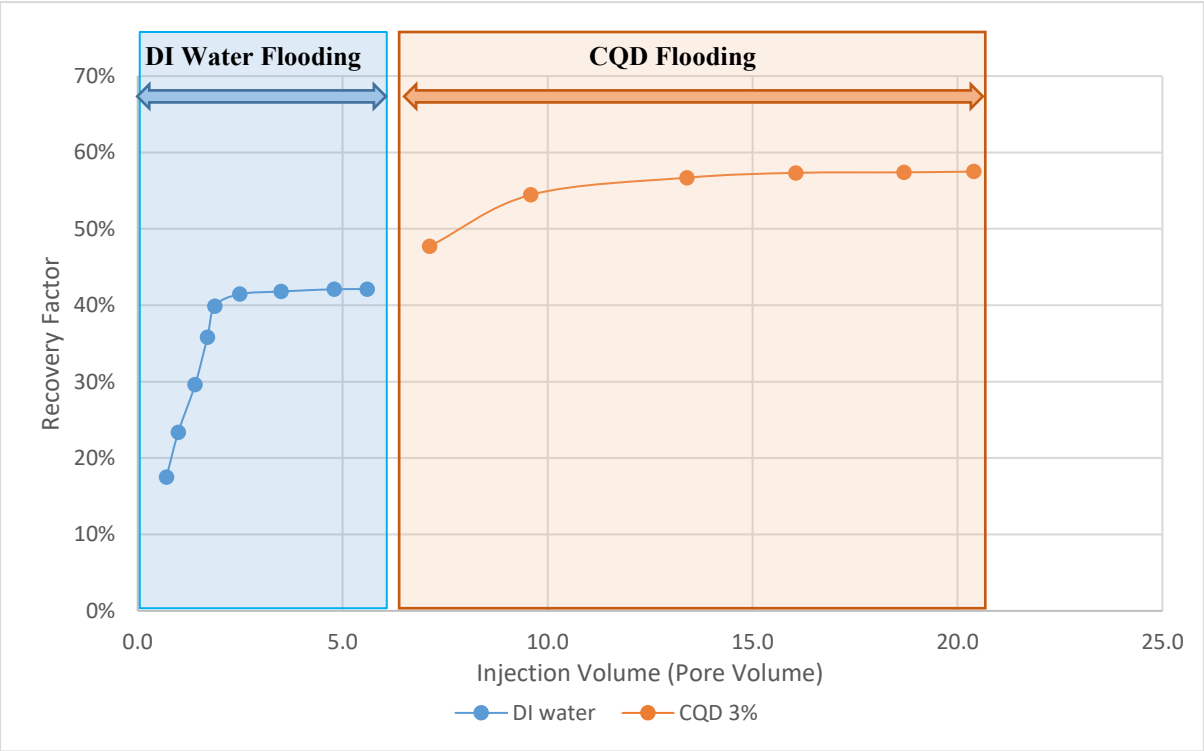


Figure 21 Recovery Factor of micromodel flooding test. Blue color area represents the recovery factor of DI water injecting; when the injected fluid is approximately 2.5 pore volume the recovery factor reaches its highest value of 41.5%. Orange color area represents the recovery factor of injecting CQD 3% that the recovery factor reaches its highest value of 57.3%.

4 Conclusions

In this study, CQDs were successfully synthesized from spent coffee grounds through a modified hydrothermal approach and evaluated as a nanofluid additive to alter the wettability and enhance oil recovery in carbonate systems. The synthesized CQDs exhibited strong blue fluorescence under UV light, confirming the successful formation of nanoscale carbon structures. Thorough investigation using XRD, FTIR, DLS, zeta potential, and FESEM analyses demonstrated the formation of stable, oxygen-functionalized carbon nanostructures with excellent aqueous dispersibility and colloidal stability. The CQDs contain tiny primary graphitic cores below 10 nm, they also maintain hydrodynamic cluster with dimensions that are smaller than typical reservoir pore throats, reducing the risk for pore plugging during transportation through porous media.

Static wettability experiments showed that CQDs are capable of altering the wettability of carbonate rock that was aged to strongly oil-wet conditions, shifting it toward water-wet conditions. At the optimal concentration of CQDs of 3 vol.%, the contact angle decreased dramatically from 123° to 52°, this confirms the strong surface activity and adsorption capability of the nanoparticles. However, by further increasing the concentration, there is a mild reversal in the wettability attitude, this is perhaps due to the aggregation of nanoparticles and the decreased interaction with the rock surface. On the contrary to these wettability changes, interfacial tension measurements showed only negligible changes.

A new manufacturing method was also developed to build strongly oil-wet glass micromodels representative of carbonate reservoir conditions. Flooding experiments carried out using the optimized 3% CQD nanofluid revealed a noticeable enhancement in oil displacement

efficiency. While DI water flooding achieved a recovery factor of 41.5%, further CQD injection increased the recovery factor to 57.3%, corresponding to an incremental recovery of approximately 15.8%. The micromodel observations showed increased oil mobilization following CQD injection, consistent with the wettability alteration observed in the static contact-angle experiments.

In summary, the results demonstrate that CQDs synthesized from spent coffee grounds can effectively alter the wettability of oil-wet carbonate surfaces and improve oil displacement in the micromodel. The use of spent coffee grounds also provides a potential route for biomass waste valorization, supporting further investigation of biomass-derived nanomaterials for more resource-efficient EOR applications.

Funding Declaration

The authors received no financial support for this research.

5 References:

1. Anderson, W.G., *Wettability literature survey - Part 1: Rock/oil/brine interactions and the effects of core handling on wettability.* Journal of Petroleum Technology, 1986.
2. Green, D.W., Willhite, G. P., *Enhanced Oil Recovery*. 1998.
3. Mohammadmoradi, P. and A. Kantzas, *Petrophysical characterization of porous media starting from micro-tomographic images.* Advances in Water Resources, 2016. **94**: p. 200-216.
4. Ahmed, T., *Reservoir engineering handbook*. 2018: Gulf professional publishing.
5. Sheng, J.J., *A comprehensive review of alkaline–surfactant–polymer (ASP) flooding.* SPE Journal, 2013.
6. Craft, B., M. Hawkins, and R. Terry, *Applied Petroleum Reservoir Engineering, seconded*. 1990, Prentice Hall.
7. Dandekar, A.Y., *Petroleum reservoir rock and fluid properties*. 2013: CRC press.
8. Sheng, J.J., *Modern Chemical Enhanced Oil Recovery: Theory and Practice*. 2011: Gulf Professional Publishing.
9. Lake, L.W., *Enhanced Oil Recovery*. 1989.
10. Abdallah, W., . and et al., *Fundamentals of wettability.* Oilfield Review, 2007.
11. Morrow, N.R., *Wettability and its effect on oil recovery.* Journal of Petroleum Technology, 1990.
12. Buckley, J. and Y. Liu, *Some mechanisms of crude oil/brine/solid interactions.* Journal of Petroleum Science and Engineering, 1998. **20**(3-4): p. 155-160.
13. Bartels, W.B., et al., *Literature review of low salinity waterflooding from a length and time scale perspective.* Fuel, 2019. **236**: p. 338-353.
14. Kumar, G., et al., *Engineering the wettability alteration of sandstone using surfactant-assisted functional silica nanofluids in low-salinity seawater for enhanced oil recovery.* ACS Engineering Au, 2022. **2**(5): p. 421-435.
15. Kuang, W., S. Saraji, and M. Piri, *A systematic experimental investigation on the synergistic effects of aqueous nanofluids on interfacial properties and their implications for enhanced oil recovery.* Fuel, 2018. **220**: p. 849-870.
16. Sharma, S. and P. Chowdhury, *Fluorescence signal from carbon quantum dots synthesized from natural resources.* Materials Today: Proceedings, 2023.

17. Yang, Z., et al., *Zero-dimensional carbon nanomaterials for fluorescent sensing and imaging.* Chemical Reviews, 2023. **123**(18): p. 11047-11136.
18. Rooj, B. and U. Mandal, *A review on characterization of carbon quantum dots.* Vietnam Journal of Chemistry, 2023. **61**(6): p. 693-718.
19. Kamal, A., S. Hong, and H. Ju, *Carbon quantum dots: synthesis, characteristics, and quenching as biocompatible fluorescent probes.* Biosensors, 2025. **15**(2): p. 99.
20. Pires, A.A., M.S. Nasser, and M.F. Mady, *Biomass-derived quantum dots for flow assurance in oil and gas–fundamentals, applications, and future outlook: a review.* Journal of Industrial and Engineering Chemistry, 2026.
21. Mirzavandi, M., et al., *Performance Evaluation of Silica–Graphene Quantum Dots for Enhanced Oil Recovery from Carbonate Reservoirs.* Energy & Fuels, 2023. **37**(2): p. 955-964.
22. Shi, X., et al., *Indoor synthesis of carbon quantum dots and its potential applications study as tracers in oilfields.* Journal of Petroleum Science and Engineering, 2022. **213**: p. 110325.
23. Sakthivel, S., et al., *Carbon nanodots for enhanced oil recovery in carbonate reservoirs.* Energy Reports, 2021. **7**: p. 8943-8959.
24. Sakthivel, S., A. Adebayo, and M.Y. Kanj, *Experimental evaluation of carbon dots stabilized foam for enhanced oil recovery.* Energy & Fuels, 2019. **33**(10): p. 9629-9643.
25. Hussain, S.S., M.S. Kamal, and M. Murtaza, *Synthesis of novel ethoxylated quaternary ammonium gemini surfactants for enhanced oil recovery application.* Energies, 2019. **12**(9): p. 1731.
26. Wu, Y., et al., *In-situ synthesis of high thermal stability and salt resistance carbon dots for injection pressure reduction and enhanced oil recovery.* Nano Research, 2023. **16**(10): p. 12058-12065.
27. Li, L., et al., *Two-step hydrothermal synthesis of active carbon-dots with high temperature and salt resistance for injection pressure reduction and enhanced oil recovery.* Colloids and Surfaces A: Physicochemical and Engineering Aspects, 2023. **676**: p. 132115.
28. Sun, Y., et al., *Carbon-Based Active Nanoparticles with Ultrahigh Temperature and Salt Resistance for Enhanced Oil Recovery from Unconventional Oil Reservoirs.* Energy & Fuels, 2023. **37**(19): p. 14882-14890.
29. Ranjbar, S., N. Sarlak, and A. Rashidi, *Fluorescent-tagged water with carbon dots derived from phenylenediamine as an equipment-free nanotracer for enhanced oil recovery.* Journal of Colloid and Interface Science, 2022. **628**: p. 43-53.
30. Gholamzadeh, Y., A. Hemmati-Sarapardeh, and M. Sharifi, *Interfacial tension reduction using nitrogen graphene quantum dots with various precursors, molar ratios, and synthesis durations for enhanced oil recovery.* Scientific Reports, 2024. **14**(1): p. 31863.
31. Saikia, T., V. Mahto, and A. Kumar, *Quantum dots: A new approach in thermodynamic inhibitor for the drilling of gas hydrate bearing formation.* Journal of industrial and engineering chemistry, 2017. **52**: p. 89-98.
32. Singh, J.P., et al., *Carbon nanoparticle synthesis, separation, characterization, and tribological property evaluation.* Separation Science and Technology, 2018. **53**(14): p. 2314-2326.
33. Kim, M.-J., et al., *Simple synthesis of spent coffee ground-based microporous carbons using K2CO3 as an activation agent and their application to CO2 capture.* Chemical Engineering Journal, 2020. **397**: p. 125404.
34. Hao, J., et al., *Carboxyl carbon quantum dots: A novel type of environmental-friendly scale inhibitor.* arXiv preprint arXiv:1810.00935, 2018.
35. Legens, C., et al., *Carbonate rock wettability changes induced by organic compound adsorption.* Journal of Petroleum science and Engineering, 1998. **20**(3-4): p. 277-282.
36. Alqam, M.H., et al., *An investigation of factors influencing carbonate rock wettability.* Energy Reports, 2021. **7**: p. 1125-1132.
37. Deng, X., et al., *A review on wettability alteration in carbonate rocks: Wettability modifiers.* Energy & Fuels, 2019. **34**(1): p. 31-54.

38. Stalder, A.F., et al., *A snake-based approach to accurate determination of both contact points and contact angles.* Colloids and surfaces A: physicochemical and engineering aspects, 2006. **286**(1-3): p. 92-103.
39. Andreas, J., E. Hauser, and W. Tucker, *Boundary tension by pendant drops1.* The Journal of Physical Chemistry, 2002. **42**(8): p. 1001-1019.
40. Daerr, A. and A. Mogne, *Pendent_drop: an imagej plugin to measure the surface tension from an image of a pendent drop.* Journal of Open Research Software, 2016. **4**(1): p. e3-e3.
41. Haynes, W.M., *CRC handbook of chemistry and physics*. 2016: CRC press.
42. Adamson, A.W. and A.P. Gast, *Physical chemistry of surfaces*. Vol. 150. 1967: Interscience publishers New York.
43. Vargaftik, N., B.N. Volkov, and L. Voljak, *International tables of the surface tension of water.* Journal of Physical and Chemical Reference Data, 1983. **12**(3): p. 817-820.
44. Romero-Zeron, L.B., *The role of porous media wettability on foamed gel propagation and fluid diverting performance.* 2005.
45. Mubari, P.K., et al., *The X-ray, Raman and TEM Signatures of Cellulose-Derived Carbons Explained.* C, 2022. **8**(1): p. 4.
46. Gan, J., et al., *Lignocellulosic Biomass-Based Carbon Dots: Synthesis Processes, Properties, and Applications.* Small, 2023. **19**(48): p. e2304066.
47. Sheshmani, S., et al., *Synthesis, optical, and photocatalytic properties of cellulose-derived carbon quantum dots.* Scientific Reports, 2025. **15**(1): p. 19027.
48. Mohammed, H.A., et al., *Sustainable hydrothermal synthesis of ultrasmall carbon quantum dots from drinking coffee and their impact on optoelectronic properties of the methyl cellulose biopolymer.* Materials Advances, 2026.
49. Scherrer, P., *Nachrichten von der Gesellschaft der Wissenschaften zu Göttingen.* Mathematisch-Physikalische Klasse, 1918. **2**(1): p. 98-100.
50. Funke, A. and F. Ziegler, *Hydrothermal carbonization of biomass: A summary and discussion of chemical mechanisms for process engineering.* Biofuels, Bioproducts and Biorefining, 2010. **4**(2): p. 160-177.
51. Coates, J., *Interpretation of Infrared Spectra, A Practical Approach*, in *Encyclopedia of Analytical Chemistry*.
52. Lua, A.C. and T. Yang, *Effect of activation temperature on the textural and chemical properties of potassium hydroxide activated carbon prepared from pistachio-nut shell.* Journal of colloid and interface science, 2004. **274**(2): p. 594-601.
53. Bhattacharjee, S., *DLS and zeta potential – What they are and what they are not?* Journal of Controlled Release, 2016. **235**: p. 337-351.
54. Stetefeld, J., S.A. McKenna, and T.R. Patel, *Dynamic light scattering: a practical guide and applications in biomedical sciences.* Biophysical Reviews, 2016. **8**(4): p. 409-427.
55. Israelachvili, J.N., *Intermolecular and surface forces*. 2011: Academic press.
56. Wong, K.C., *Review of Spectrometric Identification of Organic Compounds, 8th Edition.* Journal of Chemical Education, 2015. **92**(10): p. 1602-1603.
57. Berne, B.J. and R. Pecora, *Dynamic light scattering: with applications to chemistry, biology, and physics*. 2000: Courier Corporation.
58. Hunter, R.J., *Zeta potential in colloid science: principles and applications*. Vol. 2. 2013: Academic press.
59. Lake, L.W. and P.B. Venuto, *A niche for enhanced oil recovery in the 1990s.* Oil & Gas Journal, 1990. **88**(17): p. 62-67.
60. Sun, X., et al., *Application of nanoparticles in enhanced oil recovery: a critical review of recent progress.* Energies, 2017. **10**(3): p. 345.
61. Wang, Y. and A. Hu, *Carbon quantum dots: synthesis, properties and applications.* Journal of Materials Chemistry C, 2014. **2**(34): p. 6921-6939.

62. Roustaei, A., S. Saffarzadeh, and M. Mohammadi, *An evaluation of modified silica nanoparticles' efficiency in enhancing oil recovery of light and intermediate oil reservoirs.* Egyptian Journal of Petroleum, 2013. **22**(3): p. 427-433.
63. Baker, S.N. and G.A. Baker, *Luminescent carbon nanodots: emergent nanolights.* Angewandte Chemie International Edition, 2010. **49**(38): p. 6726-6744.
64. Ju, B., T. Fan, and M. Ma, *Enhanced oil recovery by flooding with hydrophilic nanoparticles.* China particuology, 2006. **4**(1): p. 41-46.